Hindawi
International Journal of RF and Microwave Computer-Aided Engineering
Volume 2023, Article ID 8847440, 11 pages
https://doi.org/10.1155/2023/8847440

Research Article

A Novel Broadband ± 45° Dual-Polarized Cross-Dipole Antenna with Multimode Resonance

Yanzheng Chen[1] **and Ali Raza**[2]

[1]*School of Electronic Engineering, University of Electronic Science and Technology of China, Chengdu 611731, China*
[2]*Yangtze Delta Region Institute (Huzhou), University of Electronic Science and Technology of China, Huzhou 313000, China*

Correspondence should be addressed to Yanzheng Chen; yzchen@uestc.edu.cn

Received 6 July 2023; Revised 21 August 2023; Accepted 25 August 2023; Published 9 September 2023

Academic Editor: Wen-Jun Lu

A novel broadband ± 45° dual-polarized cross-dipole antenna is presented for application in 2G, 3G, 4G, and sub-6 GHz 5G base station. A bent structure with a coplanar transmission line is used in the antenna design, which achieves multimode resonance, broadening the impedance bandwidth tremendously. Especially, it can work at $3\lambda/2$ and 2λ resonant modes without the impact of reverse current. The antenna covers the frequency spectra from 1.7 GHz to 3.8 GHz with an enhanced impedance bandwidth of roughly 76.4% and VSWRs < 1.65 at two ports. A gain of 8.3 ± 1.9 dBi and port-to-port isolation > 22.5 dB are attained in the operating frequency range. Additionally, the presented antenna has a very simple configuration and is easy to construct. A mechanical prototype of the antenna has been manufactured and measured. The experimental findings and the computational results are in good agreement.

1. Introduction

Recently, the fifth-generation (5G) mobile communication technology is developing rapidly, and many countries and regions have specified their sub-6 GHz 5G frequency bands, such as 3.4-3.8 GHz in Europe, 3.1-3.55 GHz and 3.7-4.2 GHz in the USA, and 3.3-3.6 GHz and 4.8-4.99 GHz in China [1, 2]. Unquestionably, the 5G communication technology greatly improves bandwidth shortage and the speed of wireless data transmission [3], but it has a drawback of short transmission distance. To solve this problem, the density of mobile communication base station has to be increased. Thus, the demands for base-station antennas are enhanced. In order to reduce costs, the broadband performance of the base-station antennas is pursued to cover more communication services. Many broadband dual-polarized antennas are favored in the application for the base stations [4–12].

Since the cross-dipole antenna can be easily designed as a dual-polarized antenna, numerous broadband cross-dipole antennas for application in base stations have been proposed over the years [4–7]. However, the operating frequency band of these antennas contains only 2G (1710-1920MHz), 3G (1880-2170MHz), and 4G (2300-2400MHz and 2570-2690MHz) communication bands. Thus, some academics attempt to retrofit the existing antennas by incorporating additional radiators to the principal radiator, such as loading parasitical elements above the radiator [8], using multidipoles [11], and applying shared-aperture technology [9], enabling their impedance bandwidth to encompass the sub-6 GHz 5G frequency range. Although these antennas' bandwidths have been expanded, unfortunately, these methods have enhanced the complexity of the antennas, leading to the high manufacturing cost.

In contrast to the technology of using multiradiators and loading parasitical radiators, the method of multimode resonance can expand the bandwidth of the antenna without increasing the complexity of antenna configurations [12, 13]. So far, many cross-dipole antennas have mainly been designed to work in the half-wave or full-wave modes [4–11], and the higher-order modes are less studied or used in antenna design due to the presence of reverse current

Table 1: Comparative results of the presented antenna and the same-type antennas.

Antenna	Lm (mm)	Wm (mm)	Hm (mm)	BW (GHz)	BW (%)	Gain (dBi)	Isolation (dB)	Structural complexity	Number of dielectric and grounding layers
Ref. [8]	140	140	43	1.71-2.69 (VSWR < 1.5) 3.35-3.6 (VSWR < 1.5)	NG	8.1 ± 0.4 6.6 ± 0.5	>35	Complex	2&1
Ref. [9]	140	140	36	1.60-2.70 (RL > 10) 3.28-3.80 (RL > 10) 4.75-5.18 (RL > 10)	NG	7.6 8.6 9.5	>20	Complex	3&1
Ref. [10]	105	105	30	2500-2690 (RL > 15) 3300-3600 (RL > 15)	NG	8.4 7.7	>25	Complex	5&1
Ref. [11]	106	106	39	1.7-3.22 (VSWR < 1.5)	61.8%	~ 5.7	>29	Complex	1&2
Ref. [12]	120	120	61	1.68-2.90 (RL > 10)	53.3%	6.6 ± 2.2	>34.5	Simple	NG
This work	118	118	36.8	1.7-3.8 (VSWR < 1.65)	76.4%	8.3 ± 1.9	>22.5	Simple	1&1

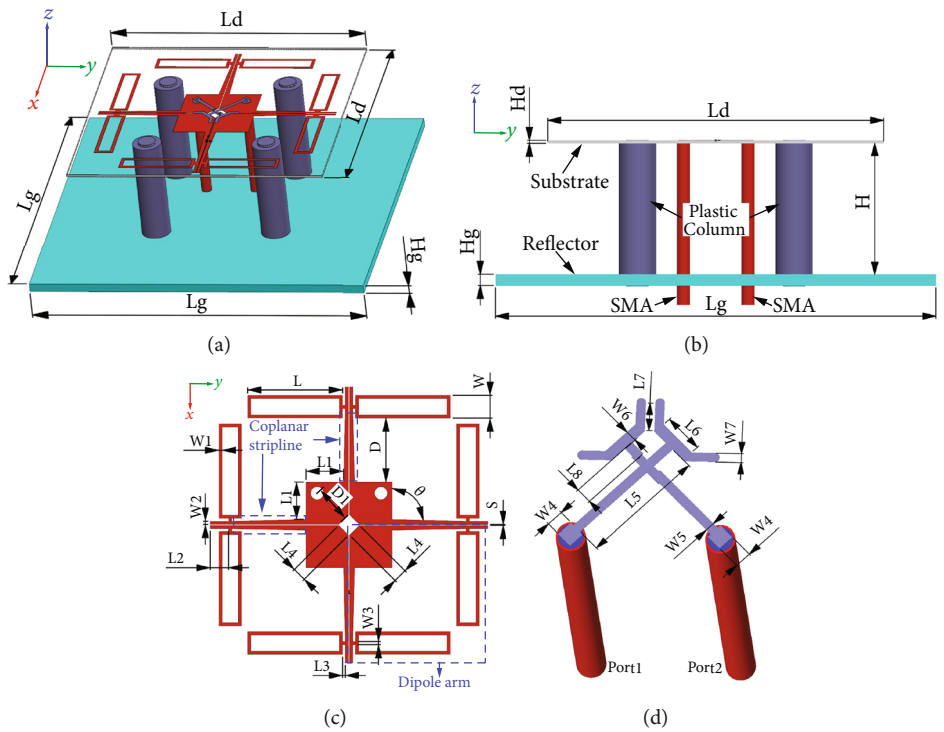

Figure 1: The presented antenna's configuration: (a) 3D view, (b) side view, (c) dipole elements, and (d) Y-shape feeding lines.

[14]. For the multimode-resonance antennas, the inclusion of the higher-order modes has great potential to increase the bandwidth of the antenna.

In this communication, we present a novel wideband ± 45° dual-polarization antenna with multimode resonance for 2G, 3G, 4G, and sub-6 GHz 5G applications. In the design of the antenna, two bent dipole elements are placed orthogonally, and one part of the dipoles forms a coplanar transmission line, which is nonradioactive and can eliminate the impact of reverse current at higher-order resonant modes. The presented dipole antenna can work at λ, $3\lambda/2$, and 2λ resonant modes with a high gain and good directional radiation patterns, and the impedance bandwidth is essentially enhanced. Table 1 compares the presented antenna with related antennas [8–12] to demonstrate its benefits. As detailed, the recommended antenna achieves a

Table 2: Structural parameters of the proposed antenna.

Parameters	Lg	Hg	Ld	Hd	H	L	W	$L1$	$W1$
Value/mm	118	2	90	0.79	34	25.9	6.5	11.4	1.1
Parameters	L2	W2	L3	W3	L4	W4	L5	W5	L6
Value/mm	5.7	0.98	0.8	2	4.5	1	14.6	1.14	4.77
Parameters	W6	L7	W7	L8	D	D1	S	θ (degree)	
Value/mm	1.36	3.35	1.09	1.94	18.6	9.8	0.24	91.4	

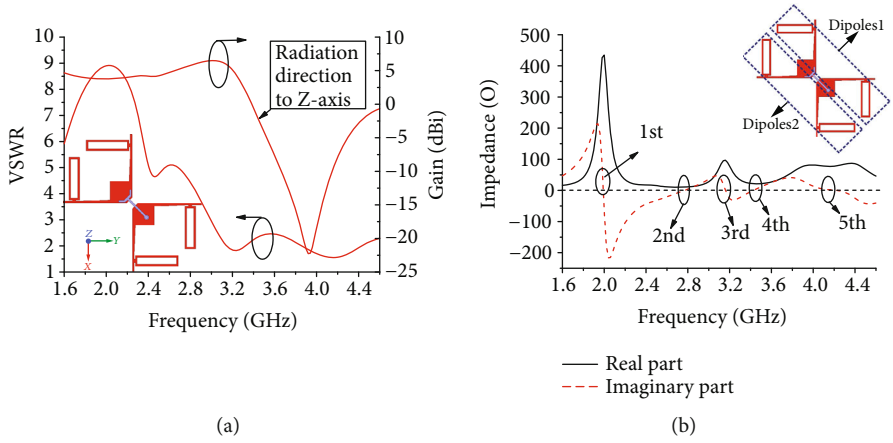

Figure 2: Impedance match and radiation gain of the proposed dipole element. (a) VSWR and gain and (b) real part and imaginary part of the input impedance.

Table 3: Comparison between the center-fed straight dipole and the presented structure at λ, $3\lambda/2$, and 2λ modes [16].

Resonant modes	Current distribution	Lobe pattern
Center-fed λ dipole	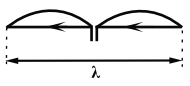	
λ resonant mode in the proposed antenna		
Center-fed $3\lambda/2$ dipole	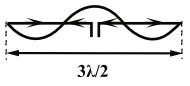	
$3\lambda/2$ resonant mode in the proposed antenna	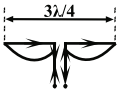	
Center-fed 2λ dipole	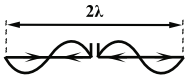	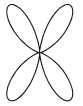
2λ resonant mode in the proposed antenna	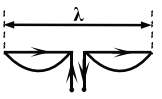	

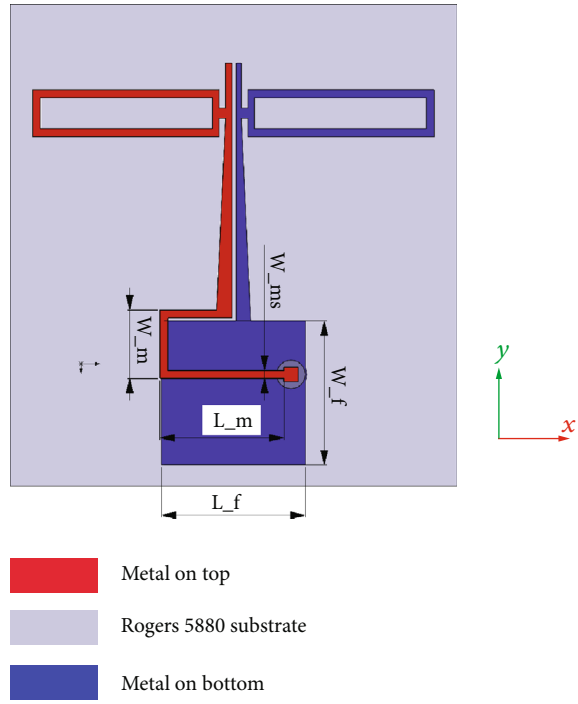

FIGURE 3: Single-polarization bent dipole with a coplanar transmission line ($L\_f = 20$ mm, $W\_f = 20$ mm, $L\_m = 17.2$ mm, $W\_m = 9.5$ mm, and $W\_ms = 2.2$ mm).

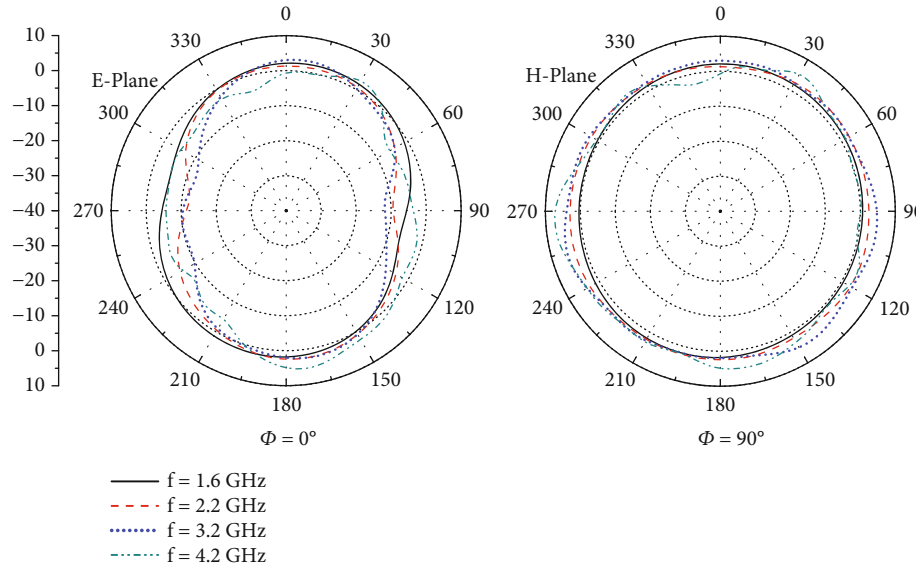

FIGURE 4: The radiation patterns of the single-polarization bent dipole.

wide impedance bandwidth and significant gain with a simple design.

2. Antenna Configuration

The configuration of the proposed antenna is described in Figure 1, and the structure-related parameters are shown in Table 2. A special structure is used as the dipole arm, which consists of two microstrip loops connected by a vertically bent microstrip line. Two dipole elements are orthogonally arranged, and one part of them forms a ladder-shaped coplanar transmission line with a slanting degree $\theta = 91.4°$. The antenna is excited using two Y-shaped feeding lines by capacitive coupling. The crossed dipoles are plated on the bottom side of a Rogers 5880 substrate with a permittivity of $\varepsilon_r = 2.2$ and a loss tangent of 0.0009, while the Y-shaped feeding lines are printed on the top side of the substrate. A portion of one Y-shaped feeding line is plated on the

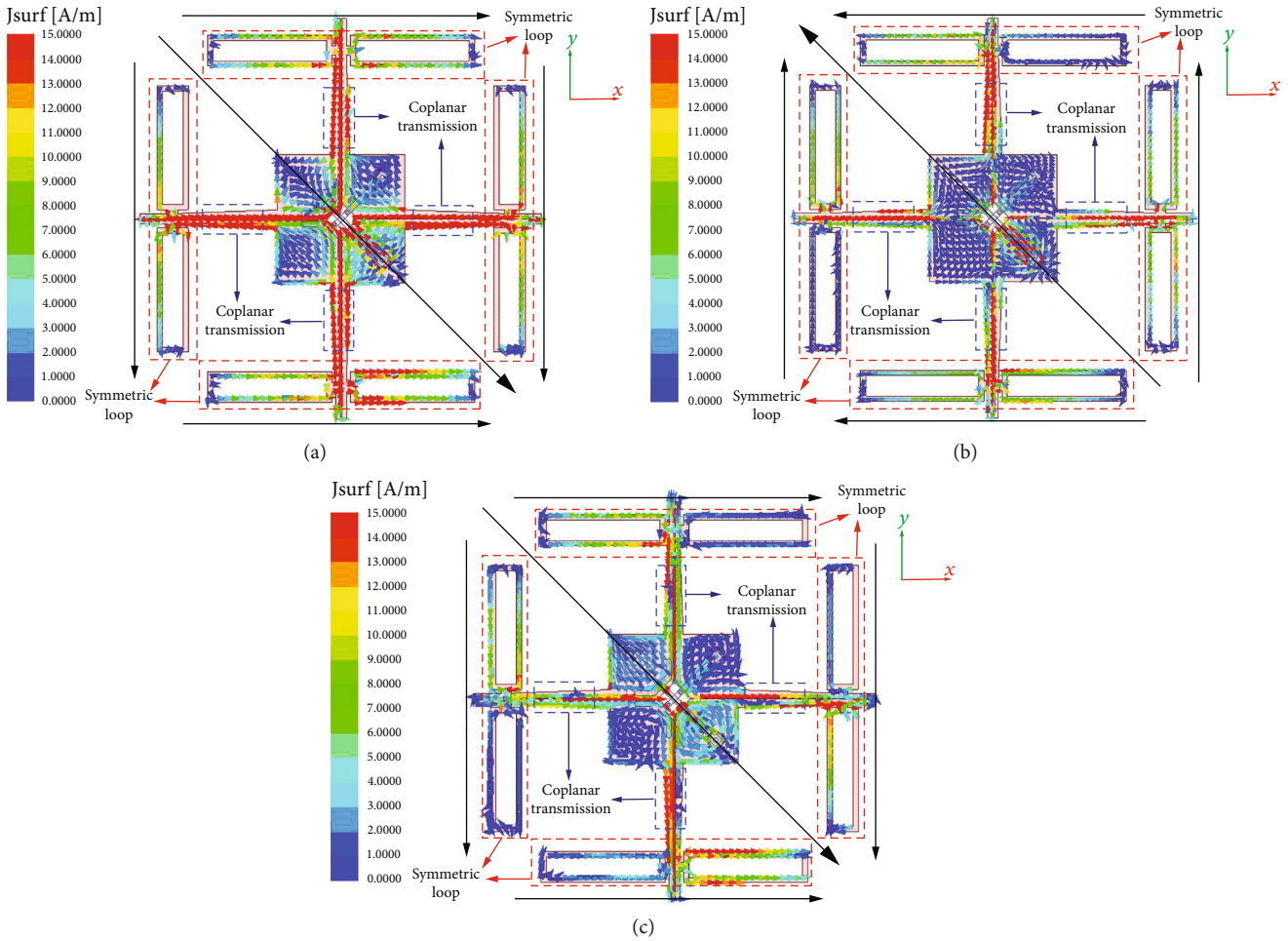

Figure 5: Current distributions on the crossed dipoles (vector value and only one port are excited). (a) 1.7 GHz, (b) 2.6 GHz, and (c) 3.6 GHz.

substrate's bottom side and connected to the top portion by shorting pins to prevent overlap. A square reflector is applied to ensure unidirectional radiation. The substrate is mounted to the reflective plate using four plastic columns, whose material and structural parameters are $\varepsilon_r = 2.1$, loss tangent = 0.001, and radius = 5 mm.

3. Antenna Principle

3.1. Analysis of Antenna Principle. Typically, the cross-dipole antennas work on the single resonant mode, and the antennas' bandwidths are mainly widened by multiple radiators. In contrast to the similar antennas, the proposed cross-dipole element resonates at multimodes, and the broad bandwidth is obtained by the multimode resonance.

The impedance match and radiation gain of the antenna with only one dipole element are shown in Figure 2. It is clear that the dipole element has a substantial radiation gain in the low-frequency range and a low radiation gain in the high-frequency region. That is, the dipole element works on the half-wave or full-wave mode in the low-frequency range, whereas it operates in higher-order modes in the high-frequency region. This can be demonstrated by calculation.

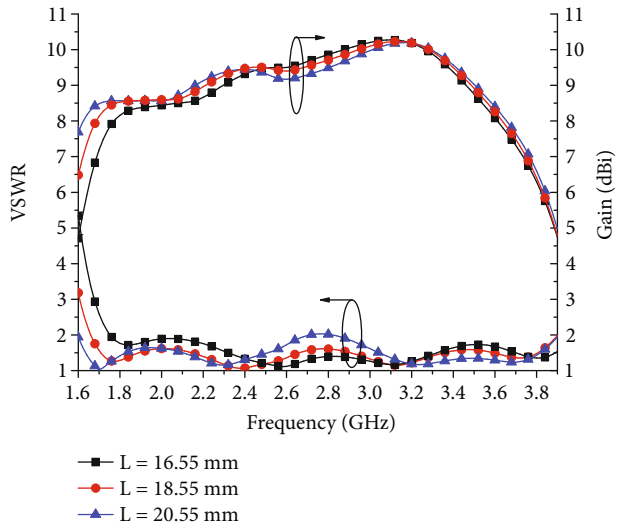

Figure 6: Effects of L on VSWR and gain.

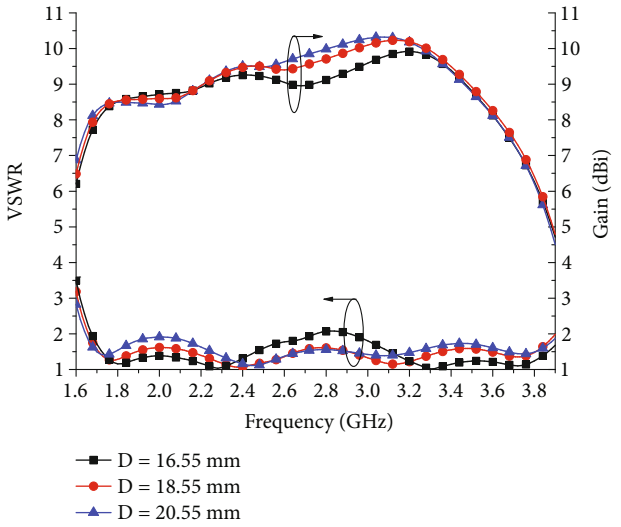

Figure 7: Effects of D on VSWR and gain.

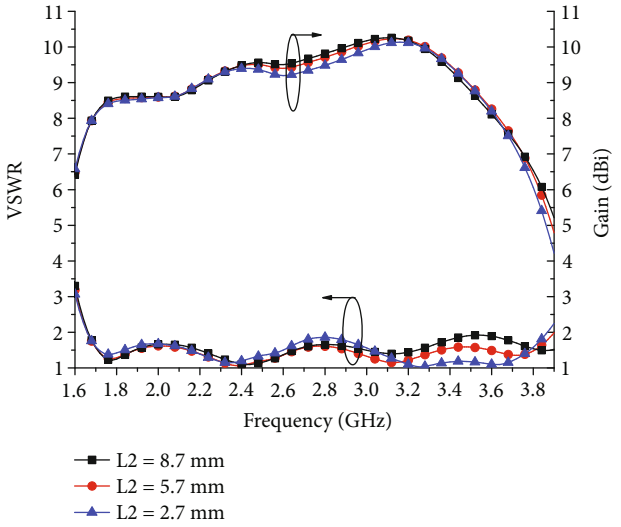

Figure 8: Effects of $L2$ on VSWR and gain.

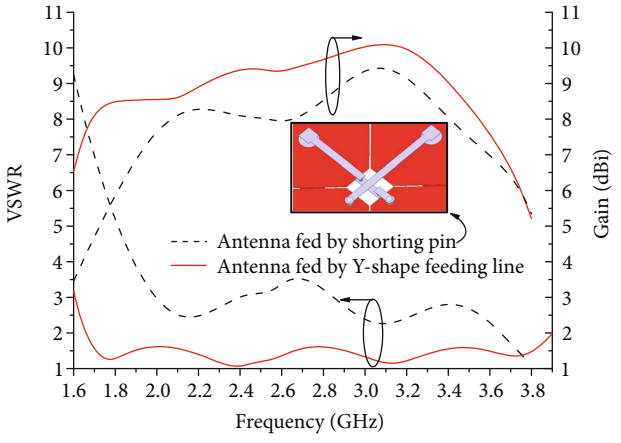

Figure 9: Comparisons of antennas fed by shorting pins and Y-shaped feeding lines.

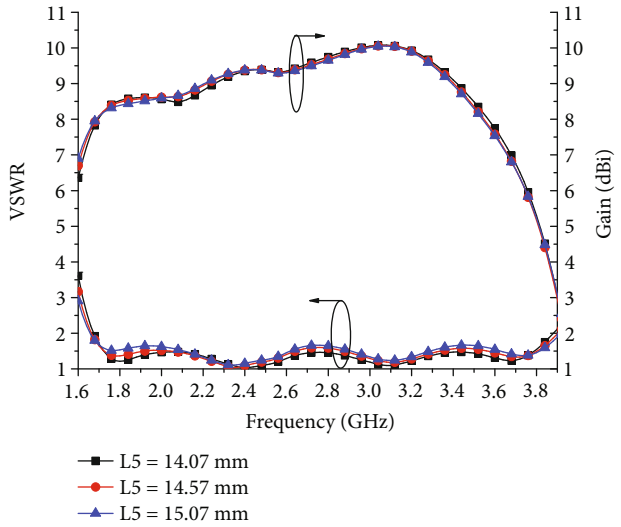

Figure 10: Effects of L5 on VSWR and gain.

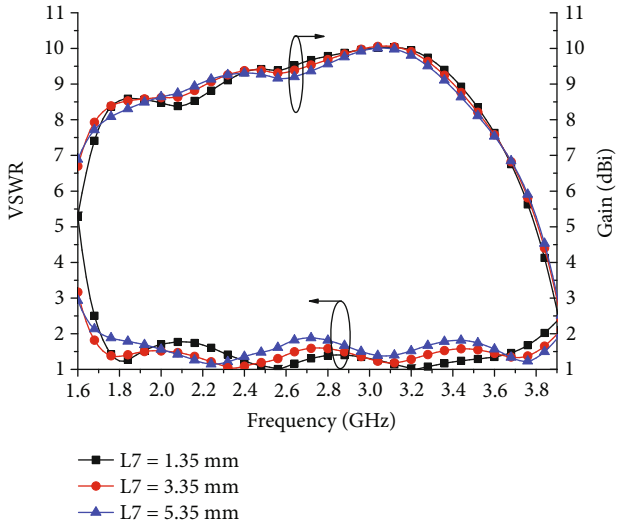

Figure 11: Effects of L7 on VSWR and gain.

As to a dipole element plated on a dielectric plate, the resonant frequency of full-wave mode can be calculated as follows [15].

$$f_\lambda = \frac{c}{l_d \times \sqrt{\varepsilon_r + 1/2}}, \quad (1)$$

where ε_r is the permittivity of the substrate and l_d indicates the dipole's length, which is about $(L + W/2 + D + L1) \times 2 = 118.2$ mm.

Based on Equation (1), the full-wave resonant frequency of the presented dipole is 2 GHz, corresponding to the low-frequency resonances in Figure 2(b). Because the dipole element can be regarded as two parallel bent dipoles, as displayed in Figure 2(b), the input impedance of the dipole element is about a half of the single dipole's one. Therefore,

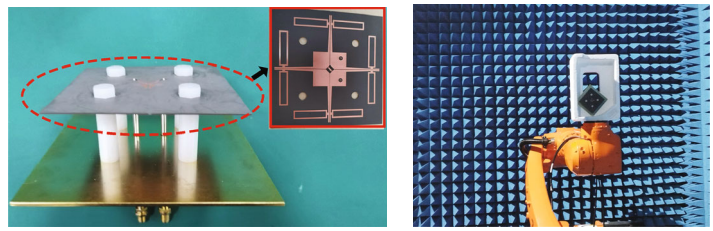

(a) (b)

Figure 12: Antenna prototype. (a) Photograph of the presented antenna. (b) Measurement scenario.

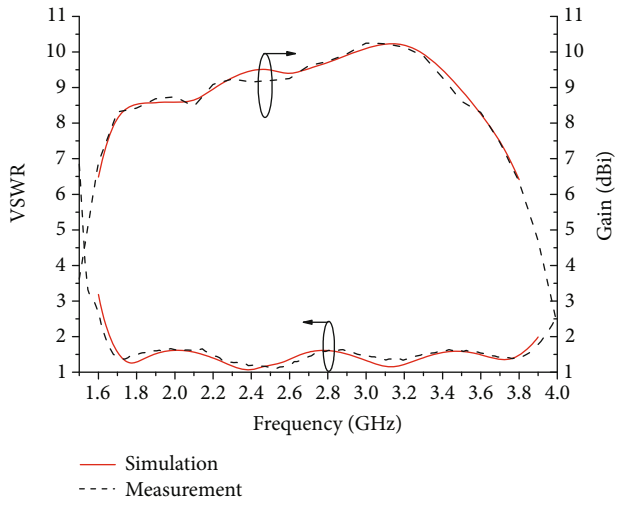

Figure 13: Simulated and measured VSWR and gain of the antenna at port 1.

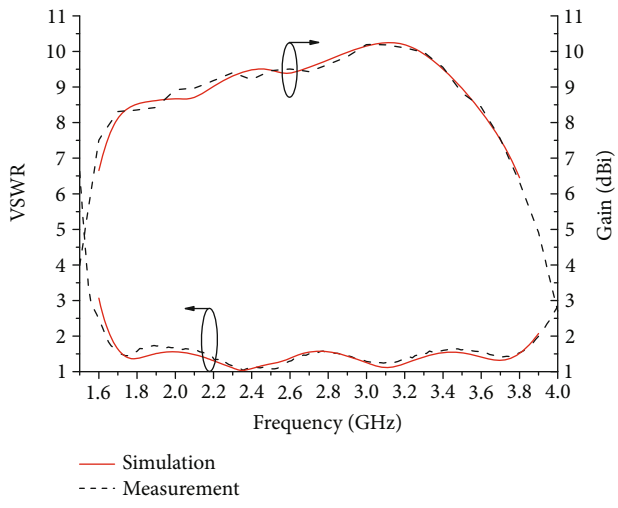

Figure 14: Simulated and measured VSWR and gain of the antenna at port 2.

the dipole element has a better impedance matching at high-order modes, which is illustrated in Figure 2(a).

To achieve dual polarization, two dipole elements are orthogonally placed. Thus, parts of the dipole elements become coplanar striplines, which can improve the antenna's low-frequency impedance match and high-frequency

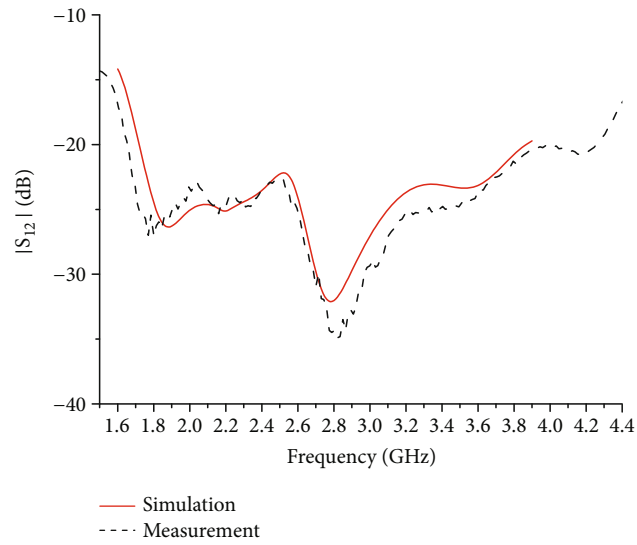

Figure 15: Simulated and measured port-to-port isolation of the antenna.

radiation gain. As tabulated in Table 3, by bending the center-fed straight dipole, the middle part of the dipole becomes a coplanar transmission line, which makes the dipole compressed. Efficiently, the λ, $3\lambda/2$, and 2λ modes are reduced to $\lambda/2$, $3\lambda/4$, and λ modes, respectively. Therefore, the proposed antenna can work at $3\lambda/2$ and 2λ resonant modes without the impact of reverse current, and the impedance bandwidths are significantly improved. As shown in Figure 3, a single-polarized bent dipole with a coplanar transmission line is investigated to verify the theory proposed in Table 3, and its radiation patterns are shown in Figure 4. The bent dipole is fed through a balun structure [17], whose structural parameters are listed in Figure 3. It is clear that the bent dipole has a figure-8 shape radiation pattern in the E-plane and a figure-O shape pattern in the H-plane in the whole working frequency band.

3.2. Current Distribution of the Presented Antenna. The current distributions on the cross-dipole antenna are presented in Figure 5. Obviously, the total current is in the direction of -45° or -225°. The feeding phase of the Y-shaped feeding lines will change with the frequencies. When the frequencies go beyond a certain bandwidth, the difference of the feeding phase reaches 180°. Therefore, in contrast with the total current at 1.7 GHz and 3.6 GHz, the one at 2.6 GHz flows in the

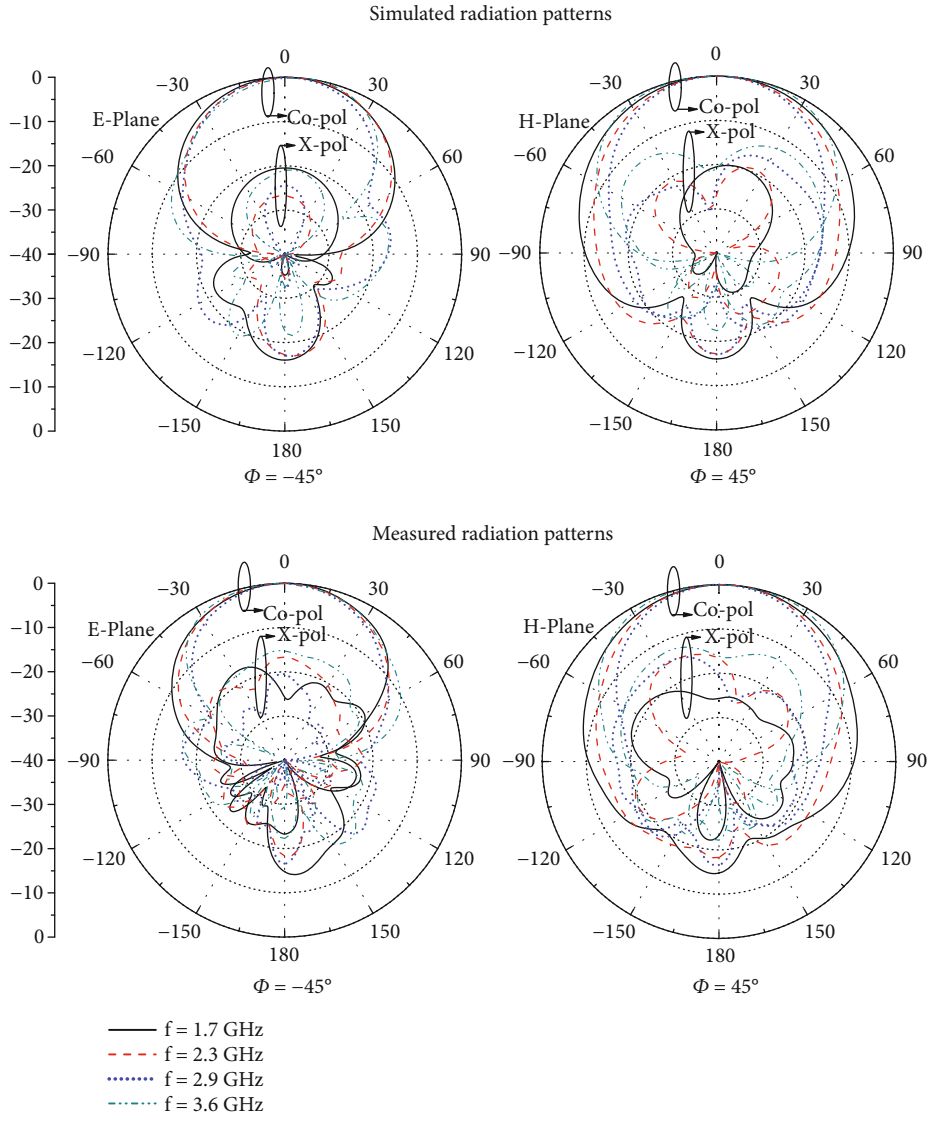

Figure 16: The radiation patterns of simulation and measurement at port 1.

opposite direction. The total current is mainly determined by the current on the symmetrical loops, and the current on the coplanar transmission lines cancels out due to the opposite direction and symmetric arrangement. Originally, although there is reverse current on the dipole element, the direction of the current on each symmetrical loop is the same. As a result, the antenna performs well in terms of radiation. When the frequency exceeds a specific threshold, such as 3.8 GHz, there is reverse current on the symmetrical loop, and it deteriorates the radiation performance of the crossed dipoles.

4. Parametric Analysis

The antenna's performance is simulated and optimized by the full-wave simulation software, which provides a useful reference for mechanical manufacturing of the antenna. The parametric analysis is implemented to show the relation between antenna's parameters and performance. For simplicity, only one port is excited, and when one parameter is analyzed, the others remain constant.

4.1. Tuning of the Resonant Modes. Essentially, these resonant frequencies are decentralized. In order to broaden the bandwidth of the antenna, parameter tunings are performed to make the resonant modes close to each other. Figures 6–8 show the effects of parameters L, D, and $L2$ on the VSWR and gain, respectively. It can be seen that the length of the symmetrical loop, L, mainly determines the resonant frequencies at both ends of the operating frequency band, while the length of the coplanar transmission lines, D, has an effect on the resonant frequencies in the middle of the operating frequency band. Additionally, the parameter $L2$ can control the resonant frequencies in the high-frequency band.

4.2. Effects of the Y-Shaped Feeding Line. The Y-shaped feeding lines have the function of enhancing the antenna's bandwidth. To investigate the role of the Y-shaped feeding lines

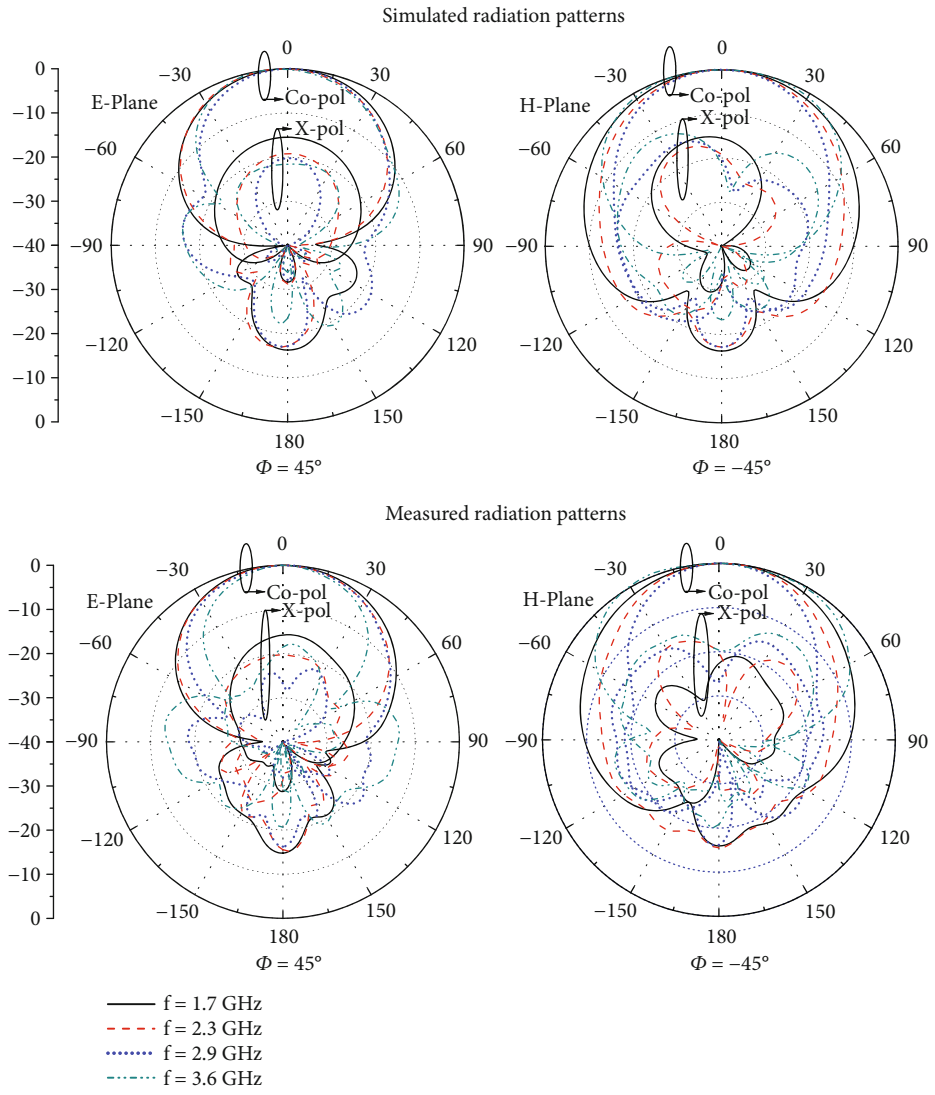

Figure 17: The radiation patterns of simulation and measurement at port 2.

in the design, a comparison between the antenna fed by shorting pins and the one excited by Y-shape feeding lines on the VSWR and gain is shown in Figure 9. It is clear that the Y-shaped feeding lines significantly enhance the antenna's impedance matching and add a resonance frequency when compared to the feeding method of shorting pins. Fed by the Y-shaped feeding lines, a capacitor is introduced, and it cancels out the inductive impedance of the dipole in the low-frequency band.

Figures 10 and 11 present the effects of the side lengths ($L5$ and $L7$) of the Y-shaped feeding lines on the performance of antenna. $L5$ and $L7$ mainly affect the impedance matching of the antenna. It can be seen that when $L5$ decreases, the antenna's VSWR in the whole frequency band is greatly improved. However, a smaller $L5$ causes two Y-shaped feeding lines to approach each other and worsens the port-to-port isolation of the antenna. Weighing the impedance matching and port-to-port isolation of the antenna, an optimal value $L5 = 14.57$ mm is chosen. The parameter $L7$ is related to the coupling intensity and location of feeding, and its change will cause the shift of the antenna's resonance frequencies. Thus, the curve of the VSWR fluctuates with the change of $L7$. After parameter optimization, $L7 = 3.35$ mm is chosen to ensure the optimal impedance matching.

5. Results and Discussion

Based on the results of the simulation, the mechanical manufacturing and measurement of the antenna are implemented to evaluate the design's efficacy. Figure 12 shows an experimental prototype of the presented antenna. The measured VSWRs and port-to-port isolation are gotten from a two-port vertical network analyzer (Agilent N5230A), and the gains are measured by a microwave anechoic chamber system.

The measurements of the VSWRs and gains at two ports, compared with the simulations, are shown in Figures 13 and 14. As can be observed, the measured findings generally match the estimates of the simulations. The constructed

Table 4: The proposed antenna's half-power beamwidths.

Frequency (GHz)	Half-power beamwidth (degree)							
	Simulation				Measurement			
	Port 1		Port 2		Port 1		Port 2	
	E-plane	H-plane	E-plane	H-plane	E-plane	H-plane	E-plane	H-plane
1.7	60.6	84.9	60.7	84.8	61	79	63	83
2	57.1	77.9	57.0	78.1	56	81	58	71
2.3	56.6	66.2	57.0	65.8	58	64	58	61
2.6	50.3	60.8	50.3	61.0	51	60	55	60
2.9	49.2	57.5	49.3	57.6	50	59	54	58
3.2	48.2	61.5	48.1	61.4	55	60	50	61
3.6	52.0	87.0	52.7	86.9	61	84	51	86

prototype's experimental results validate that the presented antenna's impedance bandwidths cover the frequency region of 1.7-3.8 GHz with VSWR < 1.65. In the working frequency band, the measured gains of 8.3 ± 1.9 dBi are obtained at two ports. Figure 15 shows the simulation and measurement of the port-to-port isolation, both of which have a high degree of similarity. The measured one is more than 22.5 dB in the operational frequency band.

At frequencies of 1.7 GHz, 2.3 GHz, 2.9 GHz, and 3.6 GHz, the simulated and measured radiation patterns, including the ones of the principal polarization and the cross polarization, are plotted in Figures 16 and 17. The experimental findings generally coincide with the simulation. Besides, the half-power beamwidths (HPBWS) of measurement and simulation are tabulated in Table 4. Because the presented antenna has a broad impedance bandwidth, the HPBWS of H-plane fluctuate greatly. For port 1, the measured HPBWs are 55.5 ± 5.5 degree at E-plane and 71.5 ± 12.5 degree at H-plane. For port 2, the measurements are 56.5 ± 6.5 degree at E-plane and 73 ± 14 degree at H-plane.

6. Conclusions

A novel ± 45° dual-polarization antenna with multimode resonance is presented for 2G, 3G, 4G, and sub-6 GHz 5G applications. The experimental findings of the constructed prototype demonstrate that the presented antenna achieves more than 76.4% impedance bandwidth from 1.7 to 3.8 GHz with VSWR < 1.65 at two ports. A gain of 8.3 ± 1.9 dBi and port-to-port isolation > 22.5 dB are obtained in the operational frequency region. The antenna achieves good performance with a very simple structure and is a prospective candidate for base station.

Data Availability

The data used to support the findings of this study are included within the article.

Conflicts of Interest

The authors declare that they have no conflicts of interest.

Acknowledgments

We thank Prof. Wenbin Lin, University of South China, for helpful discussions. This work was supported in part by the National Natural Science Foundation of China under grant nos. 11947404 and 11847307.

References

[1] W. An, Y. Li, H. Fu, J. Ma, W. Chen, and B. Feng, "Low-profile and wideband microstrip antenna with stable gain for 5G wireless applications," *IEEE Antennas and Wireless Propagation Letters*, vol. 17, no. 4, pp. 621–624, 2018.

[2] M. Li, X. Chen, A. Zhang, and A. A. Kishk, "Dual-polarized broadband base station antenna backed with dielectric cavity for 5G communications," *IEEE Antennas and Wireless Propagation Letters*, vol. 18, no. 10, pp. 2051–2055, 2019.

[3] S. X. Ta, H. Choo, and I. Park, "Broadband printed-dipole antenna and its arrays for 5G applications," *IEEE Antennas and Wireless Propagation Letters*, vol. 16, pp. 2183–2186, 2017.

[4] Q. X. Chu, D. L. Wen, and Y. Luo, "A broadband ±45° dual-polarized antenna with Y-shaped feeding lines," *IEEE Transactions on Antennas and Propagation*, vol. 63, no. 2, pp. 483–490, 2015.

[5] F. Wu and K.-M. Luk, "A reconfigurable magneto-electric dipole antenna using bent cross-dipole feed for polarization diversity," *IEEE Antennas and Wireless Propagation Letters*, vol. 16, pp. 412–415, 2017.

[6] M. Mirmozafari, G. Zhang, S. Saeedi, and R. J. Doviak, "A dual linear polarization highly isolated crossed dipole antenna for MPAR application," *IEEE Antennas and Wireless Propagation Letters*, vol. 16, pp. 1879–1882, 2017.

[7] Y. Chen, W. Lin, S. Li, and A. Raza, "A broadband ±45° dual-polarized multi-dipole antenna fed by capacitive coupling," *IEEE Transactions on Antennas and Propagation*, vol. 66, no. 5, pp. 2644–2649, 2018.

[8] S. Fu, Z. Cao, X. Quan, and C. Xu, "A broadband dual-polarized notched-band antenna for 2/3/4/5G base station," *IEEE Antennas and Wireless Propagation Letters*, vol. 19, no. 1, pp. 69–73, 2020.

[9] G.-N. Zhou, B.-H. Sun, Q.-Y. Liang, S.-T. Wu, Y.-H. Yang, and Y.-M. Cai, "Triband dual-polarized shared-aperture antenna for 2G/3G/4G/5G base station applications," *IEEE Transactions on Antennas and Propagation*, vol. 69, no. 1, pp. 97–108, 2021.

[10] Y. Liu, S. Wang, N. Li, J.-B. Wang, and J. Zhao, "A compact dual-band dual-polarized antenna with filtering structures for sub-6 GHz base station applications," *IEEE Antennas and Wireless Propagation Letters*, vol. 17, no. 10, pp. 1764–1768, 2018.

[11] Y. Feng, F.-S. Zhang, G.-J. Xie, Y. Guan, and J. Tian, "A broadband and wide-beamwidth dual-polarized orthogonal dipole antenna for 4G/5G communication," *IEEE Antennas and Wireless Propagation Letters*, vol. 20, no. 7, pp. 1165–1169, 2021.

[12] Z.-B. Zhao, W.-J. Lu, L. Zhu, and J. Yu, "Wideband wide beamwidth full-wavelength sectorial dipole antenna under dual-mode resonance," *IEEE Transactions on Antennas and Propagation*, vol. 69, no. 1, pp. 14–24, 2021.

[13] H.-H. Sun, C. Ding, H. Zhu, and Y. J. Guo, "Dual-polarized multi-resonance antennas with broad bandwidths and compact sizes for base station applications," *IEEE Open Journal of Antennas and Propagation*, vol. 1, pp. 11–19, 2020.

[14] W. J. Lu, J. Yu, and L. Zhu, "On the multi-resonant antennas: theory, history, and new development," *International Journal of RF and Microwave Computer-Aided Engineering*, vol. 29, no. 9, Article ID e21808, 2019.

[15] M. Li, M. Y. Jamal, C. Zhou, L. Jiang, and L. K. Yeung, "A novel dipole configuration with improved out-of-band rejection and its applications in low-profile dual-band dual-polarized stacked antenna arrays," *IEEE Transactions on Antennas and Propagation*, vol. 69, no. 6, pp. 3517–3522, 2021.

[16] J. D. Kraus, R. J. Marhefka, and A. S. G. Khan, *Antennas for All Applications, 3E*, McGraw-Hill Companies, New York, NY, USA, 2006.

[17] F. Farzami, S. Khaledian, B. Smida, and D. Erricolo, "Pattern-reconfigurable printed dipole antenna using loaded parasitic elements," *IEEE Antennas and Wireless Propagation Letters*, vol. 16, pp. 1151–1154, 2017.